Calcium as a nonradiative recombination center in InGaN

2017 Appl. Phys. Express 10 021001

(http://iopscience.iop.org/1882-0786/10/2/021001)

Applied Physics Express **10**, 021001 (2017)
https://doi.org/**10.7567/APEX.10.021001**

Calcium as a nonradiative recombination center in InGaN

Jimmy-Xuan Shen[1], Darshana Wickramaratne[2], Cyrus E. Dreyer[3], Audrius Alkauskas[4], Erin Young[2], James S. Speck[2], and Chris G. Van de Walle[2]

[1]*Department of Physics, University of California, Santa Barbara, CA 93106-9530, U.S.A.*
[2]*Materials Department, University of California, Santa Barbara, CA 93106-5050, U.S.A.*
[3]*Department of Physics and Astronomy, Rutgers University, Piscataway, NJ 08845-0849, U.S.A.*
[4]*Center for Physical Sciences and Technology, Vilnius LT-10257, Lithuania*

Received November 24, 2016; accepted December 19, 2016; published online January 13, 2017

Calcium can be unintentionally incorporated during the growth of semiconductor devices. Using hybrid functional first-principles calculations, we assess the role of Ca impurities in GaN. Ca substituted on the cation site acts as a deep acceptor with a level ∼1 eV above the GaN valence-band maximum. We find that for Ca concentrations of $10^{17}\,cm^{-3}$, the Shockley–Read–Hall recombination coefficient, A, of InGaN exceeds $10^{6}\,s^{-1}$ for band gaps less than 2.5 eV. A values of this magnitude can lead to significant reductions in the efficiency of light-emitting diodes.

The group-III nitrides are key materials for light-emitting diodes (LEDs).[1)] Although the internal quantum efficiency (IQE) of III–nitride LEDs in the blue region of the spectrum exceeds 90%, the efficiency in the green and yellow regions of the spectrum is much lower.[2)] Within the so-called *ABC* model, the IQE is defined as

$$\mathrm{IQE} = \frac{Bn^2}{An + Bn^2 + Cn^3}, \tag{1}$$

where A is the Shockley–Read–Hall (SRH) recombination coefficient, B is the radiative coefficient, and C is the Auger coefficient. The SRH process consists of nonradiative recombination via defect states in the band gap[3,4)] and directly affects the peak efficiency of LEDs.

The defects responsible for SRH recombination could be native point defects. For instance, gallium vacancies and their complexes have been suggested as nonradiative recombination centers in nitride LEDs,[5)] and recent computational studies have identified a microscopic mechanism by which such complexes act as SRH centers in InGaN.[6)] However, impurities should also be taken into consideration as potential sources of nonradiative recombination. Building on the recent observation that the presence of calcium is correlated with efficiency loss,[7)] we conducted a comprehensive investigation of the microscopic mechanisms by which Ca impurities cause nonradiative recombination.

Alkaline earth impurities such as calcium have previously been observed to be unintentionally incorporated during the growth of GaInNAs using molecular beam epitaxy (MBE).[8–10)] In these studies, calcium was identified through secondary ion mass spectroscopy at concentrations ranging from 10^{15} to $10^{17}\,cm^{-3}$. Wafer polishing steps were identified as the source of the unintentional Ca incorporation. It was suggested that Ca rides on the growth surface until growth conditions that support Ca incorporation occur. Calcium contamination can potentially also occur through the In source. Indium is commercially extracted as a byproduct of zinc[11)] in a process that involves leaching of zinc using sulfuric acid followed by a neutralization step using calcium carbonate. In recent work by Young et al.,[7)] Ca was found with concentrations as high as $10^{18}\,cm^{-3}$ in InGaN layers grown by ammonia MBE. The origin of the Ca was determined to be contamination on the GaN templates before MBE growth. Systematic studies showed that Ca exhibits strong surface segregation in the MBE environment.

Here we report a first-principles study of the structural and electronic properties of Ca in GaN and identify a mechanism by which Ca leads to SRH recombination in InGaN. Our calculations are based on density functional theory[12,13)] using the hybrid functional of Heyd–Scuseria–Ernzerhof[14)] (HSE), as implemented in the Vienna Ab initio Simulation Package.[15,16)] The fraction of screened Fock exchange α was set to 31%, which results in a GaN band gap of 3.48 eV, in agreement with the experimental value. A 400 eV energy cutoff was used, and spin polarization was included. The Ga d states were treated as part of the core. Impurity calculations were performed in a 96-atom GaN supercell with a $(2 \times 2 \times 2)$ Monkhorst–Pack k-point grid. The likelihood of incorporating an impurity is determined by its formation energy;[17)] for substitutional Ca on the Ga site in GaN, this is defined as

$$E^{\mathrm{form}}(\mathrm{Ca}_{\mathrm{Ga}}^{q}) = E_{\mathrm{tot}}(\mathrm{Ca}_{\mathrm{Ga}}^{q}) - E_{\mathrm{tot}}(\mathrm{GaN}) + \mu_{\mathrm{Ga}} - \mu_{\mathrm{Ca}} + q(E_{\mathrm{F}}) + \Delta^{q}, \tag{2}$$

where $E^{\mathrm{form}}(\mathrm{Ca}_{\mathrm{Ga}}^{q})$ is the total energy of the 96-atom GaN supercell with Ca on the Ga site in charge state q, $E_{\mathrm{tot}}(\mathrm{GaN})$ is the total energy of the pristine GaN supercell, and μ_{Ga} and μ_{Ca} are the chemical potentials of Ga and Ca, respectively, which depend on the growth conditions. We will show results for Ga-rich conditions (which are basically the worst case for incorporation of Ca on the Ga site) and with μ_{Ca} chosen to correspond to equilibrium with Ca_3N_2 ($\Delta H_{\mathrm{f}} = -3.95$ eV in HSE). The Fermi level (E_{F}) is referenced to the valence-band maximum (VBM) of GaN, and Δ^{q} is a finite-size correction obtained using the Freysoldt scheme.[18)]

The calculations of the nonradiative capture coefficients utilize our previously developed methodology to describe nonradiative capture of carriers by multiphonon emission.[19)] The electron–phonon matrix elements for electron and hole capture are obtained using the projector-augmented wave all-electron wavefunctions.[20)]

Three configurations of Ca impurities in GaN were considered: Ca on the Ga site ($\mathrm{Ca_{Ga}}$), Ca on the N site ($\mathrm{Ca_N}$), and Ca in an interstitial configuration ($\mathrm{Ca_i}$). The formation energies for $\mathrm{Ca_{Ga}}$, $\mathrm{Ca_N}$, and $\mathrm{Ca_i}$ are shown in Fig. 1. Substitutional Ca on the N site has a high formation energy owing to the large mismatch between the ionic radii of Ca and N; $\mathrm{Ca_N}$ is thus unlikely to be incorporated in appreciable concentrations. When calcium is incorporated as an interstitial, it is stable in the $q = 2+$ charge state across the entire

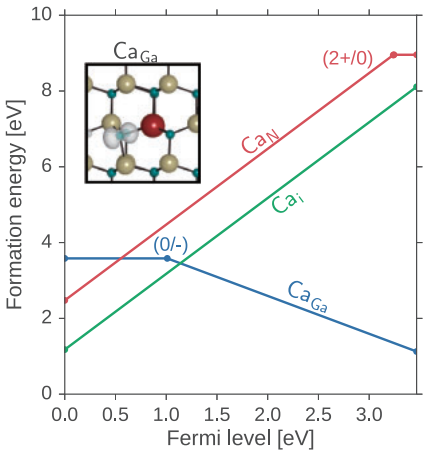

Fig. 1. Formation energy vs Fermi level for Ca_{Ga}, Ca_N, and Ca_i in various charge states under Ga-rich conditions. The atomic geometry and impurity wavefunction of neutral Ca_{Ga} are illustrated in the inset.

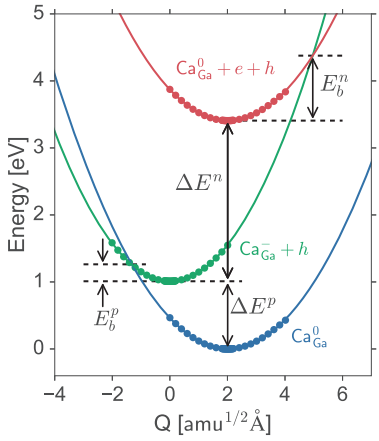

Fig. 2. Configuration coordinate diagram illustrating electron and hole capture processes. ΔE is the transition energy, and E_b is the classical barrier for the nonradiative process; the superscripts indicate whether the quantity applies to electron (n) or hole (p) capture. Solid circles denote calculated values; solid lines represent parabolic fits.

GaN band gap and thus acts as a shallow double donor. Because nonradiative captures requires a thermodynamic transition level within the gap, Ca_i does not contribute to SRH recombination.

Consistent with prior calculations,[21] we find that substitutional Ca on the Ga site acts as a deep acceptor, with a (0/—) acceptor level 1.01 eV above the VBM. The larger ionic radius of Ca compared to Ga leads to an outward relaxation of the nearest-neighbor nitrogen atoms when Ca is substituted on the Ga site. In the negative charge state, the four nearest-neighbor nitrogen atoms are uniformly displaced outward by 13% of the Ga–N bond length. In the neutral charge states, we find an asymmetric distortion of the Ca–N bonds; one of the in-plane Ca–N bonds increases by 15% of the Ga–N bond length, and the other three are increased by 12–13% of the Ga–N bond length.

We now focus on the role of Ca_{Ga} as a recombination center. A configuration coordinate diagram illustrating electron and hole capture into the (0/—) level of Ca_{Ga} is shown in Fig. 2. The transition energy ΔE (which is also called the zero-phonon line in the context of optical transitions) is given by the position of the (0/—) transition level (from Fig. 1) relative to the relevant band edge: the conduction-band minimum (CBM) for electron capture, leading to a transition energy ΔE^n, and the VBM for hole capture, leading to a transition energy ΔE^p.

A complete recombination cycle requires capture of an electron by the neutral impurity, followed by capture of a hole by the negatively charged impurity. The overall recombination rate is thus governed by the *slower* of the two processes. The nonradiative capture rate decreases roughly exponentially with the energy of the transition.[22] In GaN, the (0/—) level of Ca_{Ga} is much closer to the VBM, and therefore the nonradiative capture coefficient for holes, C_p, is expected to be orders of magnitude larger than that for electrons, C_n. Slow electron capture will thus limit the SRH recombination rate for Ca_{Ga} in GaN.

The situation is dramatically different in InGaN, which constitutes the active layer in visible LEDs. As the In content of InGaN increases, the band gap decreases; we now examine how the position of the Ca_{Ga} (0/—) level shifts with respect to the band edges as a function of In content. We continue

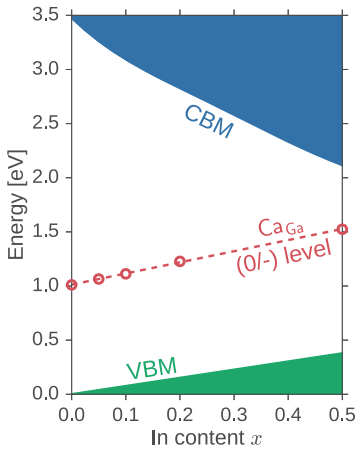

Fig. 3. Calculated position of the (0/—) transition level of Ca_{Ga} within the band gap of InGaN as a function of In content.

to use the notation "Ca_{Ga}" as a generic designation for incorporation of Ca on a group-III site in the InGaN alloy. We follow the procedure outlined in Ref. 6, where it was shown that the primary effect on the defect level is due to the lattice expansion that occurs with increasing In content of the alloy. We thus calculate the thermodynamic transition level for Ca_{Ga} using lattice parameters corresponding to InGaN alloys with In contents of 5, 10, and 25%. To apply this information to actual InGaN alloys, we align the VBM in the expanded cell with that of unstrained GaN using the absolute valence-band deformation potential of GaN.[23] The band edges in the InGaN alloy, again aligned with respect to unstrained GaN, are taken from Ref. 24.

The results are shown in Fig. 3. We observe that the energy difference between the (0/—) level and the CBM is indeed significantly reduced in InGaN alloys.

Using these results, we now determine the nonradiative electron and hole capture coefficients for Ca_{Ga} as a function of In content. The capture coefficients, C_n and C_p, are shown as a function of the band gap of the InGaN alloy in Fig. 4, assuming a typical internal operating temperature of 390 K. Because the (0/—) transition level increases only slightly with respect to the VBM of InGaN (Fig. 3), the hole capture

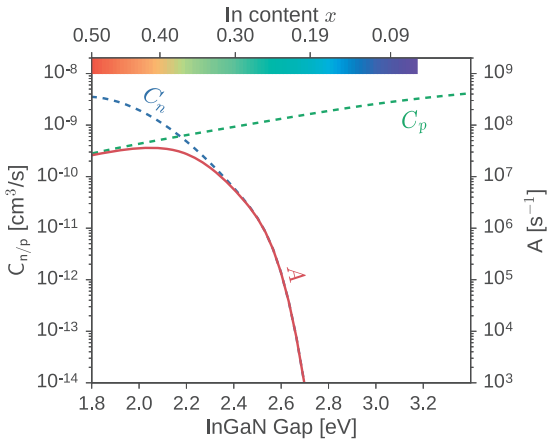

Fig. 4. Electron (C_n) and hole (C_p) capture coefficients for the (0/—) level of Ca_{Ga} in InGaN calculated at 390 K. The SRH coefficient, A, is calculated for a Ca density of $10^{17}\,cm^{-3}$.

coefficient, C_p, does not change dramatically over the plotted range. For electron capture, the transition energy decreases rapidly with increasing indium content, resulting in a dramatic rise in C_n.

At a given impurity density N, the SRH recombination rate is characterized by the A coefficient, where

$$A = N\frac{C_n C_p}{C_n + C_p}. \quad (3)$$

The coefficient A calculated for a Ca impurity concentration of $N = 10^{17}\,cm^3$ is also shown in Fig. 4. The figure shows that at low In content (large band gap), the rate-limiting step is electron capture, whereas at higher In content (low band gap), hole capture limits the rate. This crossover is directly related to the position of the Ca_{Ga} (0/—) level within the band gap. As the In content increases, the energy difference between the CBM and the (0/—) level decreases more rapidly than the slight increase in the energy difference between the VBM and the (0/—) level occurs (Fig. 3).

We can now assess the impact of unintentional Ca incorporation on the IQE of an LED, again assuming $N = 10^{17}\,cm^3$. To do so, we compare the rate of nonradiative SRH recombination, An, with the rate of radiative band-to-band transitions, Bn^2, or, alternatively, the magnitude of A with the magnitude of Bn. We assume an operating carrier density of $n = 10^{18}\,cm^{-3}$. The recombination coefficient in an InGaN quantum well is given by $B = 4\times10^{-11}\,cm^3\,s^{-1}$,[25] (since B depends weakly on the In content, we use the value for $x = 0.25$), and hence $Bn = 4\times10^7\,cm^{-3}\,s^{-1}$. Figure 4 shows that in the blue region of the spectrum, the A coefficient is sufficiently low that it does not cause loss of carriers. However, as the In content increases and the band gap decreases toward the green region of the spectrum, the A coefficient increases significantly; for a band gap of 2.3 eV, the SRH coefficient is approximately $10^7\,s^{-1}$. Comparing this value with Bn, we conclude that 20% of the carriers would be lost because of SRH recombination. Control of Ca during nitride growth is thus very important. The study by Young et al.[7] showed that alternating high-temperature/low-temperature MBE layers can effectively incorporate Ca in the low-temperature layers and thus reduce the Ca concentration in the active layer to as low as $10^{14}\,cm^{-3}$.

In conclusion, we used first-principles calculations to determine the thermodynamic transition levels and nonradiative recombination properties of Ca in GaN. We found that Ca_{Ga} behaves as a deep acceptor with a level ~1 eV above the GaN VBM. For a Ca impurity concentration of $10^{17}\,cm^{-3}$, we found SRH coefficients exceeding $10^6\,s^{-1}$ for InGaN band gaps below 2.5 eV. SRH coefficients of this magnitude can severely limit the IQE of nitride LEDs.[26]

Acknowledgments J.S., D.W., and C.V.d.W were supported by the U.S. Department of Energy (DOE), Office of Science, Basic Energy Sciences (BES) under Award No. DE-SC0010689. A.A. was supported by the Marie Sklodowska-Curie Action of the European Union (Project Nitride-SRH, Grant No. 657054). E.Y. and J.S.S. were supported by the KACST-KAUST-UCSB Solid State Lighting Program. Additional support was provided by the National Science Foundation IMI Program (Grant No. DMR08-43934). Computational resources were provided by the National Energy Research Scientific Computing Center, which is supported by the DOE Office of Science under Contract No. DE-AC02-05CH11231.

1) S. Nakamura and M. R. Krames, Proc. IEEE **101**, 2211 (2013).
2) K. A. Bulashevich, A. V. Kulik, and S. Y. Karpov, Phys. Status Solidi A **212**, 914 (2015).
3) W. Shockley and W. T. Read, Phys. Rev. **87**, 835 (1952).
4) R. N. Hall, Phys. Rev. **87**, 387 (1952).
5) S. F. Chichibu, A. Uedono, T. Onuma, T. Sota, B. A. Haskell, S. P. DenBaars, J. S. Speck, and S. Nakamura, Appl. Phys. Lett. **86**, 021914 (2005).
6) C. E. Dreyer, A. Alkauskas, J. L. Lyons, J. S. Speck, and C. G. Van de Walle, Appl. Phys. Lett. **108**, 141101 (2016).
7) E. C. Young, N. Grandjean, T. E. Mates, and J. S. Speck, Appl. Phys. Lett. **109**, 212103 (2016).
8) A. J. Ptak, D. J. Friedman, S. Kurtz, R. C. Reedy, M. Young, D. B. Jackrel, H. B. Yuen, S. R. Bank, M. A. Wistey, and J. S. Harris, J. Vac. Sci. Technol. B **24**, 1540 (2006).
9) J. B. Hurst, S. D. Lewis, M. M. Oye, A. L. Holmes, A. J. Ptak, and R. C. Reedy, J. Vac. Sci. Technol. B **25**, 1058 (2007).
10) M. M. Oye, S. R. Bank, A. J. Ptak, R. C. Reedy, M. S. Goorsky, and A. L. Holmes, J. Vac. Sci. Technol. B **26**, 1058 (2008).
11) A. Alfantazi and R. Moskalyk, Miner. Eng. **16**, 687 (2003).
12) P. Hohenberg and W. Kohn, Phys. Rev. **136**, B864 (1964).
13) W. Kohn and L. J. Sham, Phys. Rev. **140**, A1133 (1965).
14) J. Heyd, G. E. Scuseria, and M. Ernzerhof, J. Chem. Phys. **124**, 219906 (2006).
15) G. Kresse and J. Furthmüller, Phys. Rev. B **54**, 11169 (1996).
16) G. Kresse and J. Furthmüller, Comput. Mater. Sci. **6**, 15 (1996).
17) C. Freysoldt, B. Grabowski, T. Hickel, J. Neugebauer, G. Kresse, A. Janotti, and C. G. Van de Walle, Rev. Mod. Phys. **86**, 253 (2014).
18) C. Freysoldt, J. Neugebauer, and C. G. Van de Walle, Phys. Rev. Lett. **102**, 016402 (2009).
19) A. Alkauskas, Q. Yan, and C. G. Van de Walle, Phys. Rev. B **90**, 075202 (2014).
20) P. E. Blöchl, Phys. Rev. B **50**, 17953 (1994).
21) J. Neugebauer and C. G. Van de Walle, J. Appl. Phys. **85**, 3003 (1999).
22) A. M. Stoneham, *Theory of Defects in Solids* (Oxford University Press, Oxford, U.K., 2001).
23) C. G. Van de Walle and J. Neugebauer, Appl. Phys. Lett. **70**, 2577 (1997).
24) P. G. Moses and C. G. Van de Walle, Appl. Phys. Lett. **96**, 021908 (2010).
25) E. Kioupakis, Q. Yan, D. Steiauf, and C. G. Van de Walle, New J. Phys. **15**, 125006 (2013).
26) J. Danhof, U. T. Schwarz, T. Meyer, C. Vierheilig, and M. Peter, Phys. Status Solidi B **249**, 600 (2012).